



Babeş-Bolyai University  
Faculty of Chemistry and Chemical Engineering  
Doctoral School of Chemistry



## **Doctoral thesis**

# **SYNTHESIS AND CHARACTERIZATION OF NEW PHENOTHIAZINE DERIVATIVES FOR FUNCTIONAL DYE**

**Scientific Coordinator**

**Prof. Dr. Habil. Radu-Lucian Silaghi-Dumitrescu**

**Phd student**

**Gal Melinda-Éva**

**Cluj-Napoca**

**2024**

**Keywords:** salts of 10-ethyl-10H-phenothiazine-3-carboxylated acid, mechano-chemical synthesis, nanomaterials, electrospinning, latent fingerprints, sensor for explosives, N-arylamino fenazationium dyes, optical properties.

## CONTENTS OF THE DOCTORAL THESIS

### Contents

Summary .....	Hiba! A könyvjelző nem létezik.
<b>CHAPTER 1: Synthesis of salts of 10-ethyl-10H-phenothiazine-3-carboxylic acid</b>	<b>Hiba! A könyvjelző nem létezik.</b>
1.1. Introduction .....	Hiba! A könyvjelző nem létezik.
1.2. Results and discussions .....	Hiba! A könyvjelző nem létezik.
1.2.1. Synthesis of 10-alkyl-10H-phenothiazine-3-carboxylic acid ...	Hiba! A könyvjelző nem létezik.
1.2.2. Salt synthesis of 10-ethyl-10H-phenothiazine-3-carboxylic acid	Hiba! A könyvjelző nem létezik.
1.2.3. Structural characterization.....	Hiba! A könyvjelző nem létezik.
1.2.3.1. Study of MRI spectra.....	Hiba! A könyvjelző nem létezik.
1.2.3.2. Single-crystal X-ray diffraction .....	Hiba! A könyvjelző nem létezik.
1.2.3.2.1. Lithium salt of 10-ethyl-10H-phenothiazine-3-carboxylic acid (3a) .....	Hiba! A könyvjelző nem létezik.
1.2.3.2.2. Sodium salt of acid 10-ethyl-10H-phenothiazine-3-carboxylic (3b).....	Hiba! A könyvjelző nem létezik.
1.2.3.2.3. Potassium salt of acid 10-ethyl-10H-phenothiazine-3-carboxylic (3c).....	Hiba! A könyvjelző nem létezik.
1.2.3.2.4. Calcium salt of acid 10-ethyl-10H-phenothiazine-3-carboxylic (3d) .....	Hiba! A könyvjelző nem létezik.
1.2.3.2.5. Rubidium salt of 10-ethyl-10H-phenothiazine-3-carboxylic acid (3f).....	Hiba! A könyvjelző nem létezik.
1.2.3.2.6. Cesium salt of acid 10-ethyl-10H-phenothiazine-3-carboxylic (3g).....	Hiba! A könyvjelző nem létezik.
1.2.3.3. Study of electronic properties .....	Hiba! A könyvjelző nem létezik.
1.2.3.3.1. UV-Vis Absorption Spectroscopy.....	Hiba! A könyvjelző nem létezik.
1.2.3.3.2. Fluorescence emission spectroscopy in solution	Hiba! A könyvjelző nem létezik.
1.2.3.3.3. Fluorescence Emission Spectroscopy in Solid...	Hiba! A könyvjelző nem létezik.
1.2.4. Obtaining fluorescent nanomaterials by electrospinning	Hiba! A könyvjelző nem létezik.

- 1.2.4.1. Characterization of nanomaterials..... Hiba! A könyvjelző nem létezik.**
- 1.2.4.1.1. Characterization of nanomaterials by transmission electron microscopy (TEM)**Hiba! A könyvjelző nem létezik.**
- 1.2.4.1.2. Characterization of nanomaterials by scanning or scanning electron microscopy (SEM) **Hiba! A könyvjelző nem létezik.**
- 1.2.4.1.3. Characterization of phenothiazine carboxylates 3a-g and nanomaterials by fluorescence imaging microscopy (FLIM) ..... **Hiba! A könyvjelző nem létezik.**
- 1.2.4.1.4. Analysis of fluorescence emission properties of nanomaterials obtained by electrospinning functionalized with 3a-f salts, in solid state. **Hiba! A könyvjelző nem létezik.**
- 1.2.5. Practical applications ..... Hiba! A könyvjelző nem létezik.**
- 1.2.5.1. Detection of traces of latent papillary prints on different surfaces ..... Hiba! A könyvjelző nem létezik.**
- 1.2.5.1.1. Procedure for detecting papillary traces..... **Hiba! A könyvjelző nem létezik.**
- 1.2.5.1.2. Detection Efficiency..... **Hiba! A könyvjelző nem létezik.**
- 1.2.5.1.3. Stability of papillary trace images taken on nanomaterials**Hiba! A könyvjelző nem létezik.**
- 1.2.5.1.4. Detection of papillary traces with aged nanomaterials ... **Hiba! A könyvjelző nem létezik.**
- 1.2.5.2. Explosive Substance Detection..... Hiba! A könyvjelző nem létezik.**
- 1.2.5.2.1. Detection mechanism ..... **Hiba! A könyvjelző nem létezik.**
- 1.2.5.2.2. Manufacture of fluorescent sensors for the detection of nitroderivatives .. **Hiba! A könyvjelző nem létezik.**
- 1.3. Materials and methods..... Hiba! A könyvjelző nem létezik.**
- 1.3.1. Synthesis of 10-ethyl-3-carboxy phenothiazine using silver oxideHiba! A könyvjelző nem létezik.**
- 1.3.2. Synthesis of salts of 10-ethyl-10Hphenothiazine-3-carboxylic acidHiba! A könyvjelző nem létezik.**
- 1.3.2.1. General method of preparation of salts of 10-ethyl-10H 3-carboxy phenothiazine-3-carboxylic acid ..... **Hiba! A könyvjelző nem létezik.**
- 1.3.2.2. General method of preparation of salts of 10-ethyl-10H 3-carboxy phenothiazine-3-carboxylic acid with carbonate..... **Hiba! A könyvjelző nem létezik.**
- 1.3.2.3. Mechanochemical method of obtaining salts of 10-ethyl-10H 3-carboxy phenothiazine-3-carboxylic acid..... **Hiba! A könyvjelző nem létezik.**
- 1.3.3. Synthesis of Zn(OH) nanoparticles<sub>2</sub> using the precipitation method. Hiba! A könyvjelző nem létezik.**
- 1.3.4. Preparation of polymer solutions for electrospinning.... Hiba! A könyvjelző nem létezik.**
- 1.3.5. Obtaining FLIM images..... Hiba! A könyvjelző nem létezik.**

1.3.6. Method of obtaining sensors for explosives containing aromatic nitroderivatives	Hiba! A könyvjelző nem létezik.
1.4. Conclusions .....	22
<b>CHAPTER 2 : Synthesis of new dyes derived from N-arilamino fenazationium</b>	
Hiba! A könyvjelző nem létezik.	
2.1. Introduction .....	Hiba! A könyvjelző nem létezik.
2.2. Results and discussions .....	Hiba! A könyvjelző nem létezik.
2.2.1. Synthesis of new dyes derived from N-arilamino fenazationium	Hiba! A könyvjelző nem létezik.
2.2.2. Structural characterisation.....	Hiba! A könyvjelző nem létezik.
2.2.2.1. Study of MRI and HRMS spectra.....	Hiba! A könyvjelző nem létezik.
2.2.2.3. Single-crystal X-ray diffraction.....	Hiba! A könyvjelző nem létezik.
2.2.2.3.1. Determination of the crystal structure of dye 2a ...	Hiba! A könyvjelző nem létezik.
2.2.2.3.2. Determination of the crystal structure of the dye 2f-Cl <sup>-</sup> and 2f-I	Hiba! A könyvjelző nem létezik.
2.2.2.3. Study of electronic properties.....	Hiba! A könyvjelző nem létezik.
2.2.2.3.1. UV-Vis spectroscopy: aggregation and solvatochromia studies	Hiba! A könyvjelző nem létezik.
2.2.3. Characterization of 4b-f dyes by FLIM imaging .....	Hiba! A könyvjelző nem létezik.
2.2.4. Aggregation study of 2b-2g dyes .....	Hiba! A könyvjelző nem létezik.
2.2.5. Lipophilicity study .....	Hiba! A könyvjelző nem létezik.
2.2.6. Practical applications .....	Hiba! A könyvjelző nem létezik.
2.2.6.1. Explosive Substance Detection.....	Hiba! A könyvjelző nem létezik.
2.2.6.1.1. Detection mechanism .....	Hiba! A könyvjelző nem létezik.
2.2.6.1.2. Manufacture of sensors for the detection of nitroderivatives	Hiba! A könyvjelző nem létezik.
2.2.6.2. Applications in selective staining of cells .....	Hiba! A könyvjelző nem létezik.
2.3. Materials and methods.....	Hiba! A könyvjelző nem létezik.
2.3.1. General synthesis of new N-arylamino-phenothiazinium dyes ..	Hiba! A könyvjelző nem létezik.
2.3.2. General Procedure for Ultrasonic Irradiation Synthesis of N-Arylamino-Phenothiazinium Derived Dyes .....	Hiba! A könyvjelző nem létezik.
2.3.2.1. Ultrasonic indirect irradiation procedure .....	Hiba! A könyvjelző nem létezik.
2.3.2.2. Direct ultrasonic irradiation procedure .....	Hiba! A könyvjelző nem létezik.
2.3.3. Mechanochemical synthesis.....	Hiba! A könyvjelző nem létezik.

2.3.4. General procedure for obtaining 3,7-diarilamino-3H-phenothiazine	Hiba! A könyvjelző nem létezik.
2.3.5. Lipophilicity Protocol.....	Hiba! A könyvjelző nem létezik.
2.3.5. Getting the Sensor .....	Hiba! A könyvjelző nem létezik.
2.4. Conclusions .....	30
References .....	Hiba! A könyvjelző nem létezik.
LIST OF PUBLICATIONS AND PARTICIPATION IN CONFERENCES	Hiba! A könyvjelző nem létezik.
Annex.....	Hiba! A könyvjelző nem létezik.

## CONTENTS OF THE DOCTORAL ABSTRACT

Summary .....	6
CHAPTER 1: Synthesis of salts of 10-ethyl-10H-phenothiazine-3-carboxylic acid .....	6
1.1 Introduction .....	7
1.2 Results and discussions .....	8
1.2.1. Salt synthesis of 10-ethyl-10H-phenothiazine-3-carboxylic acid .....	8
1.2.2. Structural characterisation.....	9
1.2.2.1. Study of NMR spectra.....	9
1.2.2.2. X-ray diffraction on single crystal .....	10
1.2.2.3. Study of electronic properties.....	11
1.2.2.3.1. UV-Viz absorption spectroscopy.....	11
1.2.2.3.2. Fluorescence emission spectroscopy in solution .....	13
1.2.3. Obtaining fluorescent nanomaterials by electrospinning .....	15
1.1.1.1. Characterization of nanomaterials .....	15
1.1.1.1.1. Characterization of nanomaterials by transmission electron microscopy (TEM) ....	15
1.1.1.1.2. Characterization of nanomaterials by scanning or scanning electron microscopy (SEM)	16
1.1.1.1.3. Characterization of phenothiazine carboxylates 3a-g and nanomaterials by fluorescence imaging microscopy (FLIM) .....	17
1.2.4. Practical applications .....	18
1.2.4.1. Detection of traces of latent papillary prints on different surfaces.....	18
1.2.4.1.1. Procedure for detecting papillary traces .....	18

1.2.4.2. Explosive Substance Detection .....	20
1.3. Conclusions .....	22
CHAPTER 2 : Synthesis of new dyes derived from N-arilamino fenazationium .....	23
2.1. Introduction .....	23
2.2. Results and discussions .....	23
2.2.1. Synthesis of new dyes derived from N-arilamino fenazationium .....	23
2.2.2. Structural characterisation.....	24
2.2.2.1. Study of MRI and HRMS spectra.....	24
2.2.2.2. X-ray diffraction on single crystal .....	25
2.2.2.3. Study of electronic properties.....	26
2.2.3. Characterization of 4b-f dyes by FLIM imaging.....	27
2.2.4. Practical applications .....	27
2.2.4.1. Explosive Substance Detection .....	27
2.2.4.2. Applications in selective staining of cells.....	29
2.3. Conclusions .....	30
References .....	31

## Summary

The thesis includes the synthesis and characterisation of new phenothiazine derivatives and their applicability in medical and forensic fields.

The first chapter of the thesis includes the development of new synthetic procedures to obtain new salts of 10-ethyl-10H-phenothiazine-3-carboxylic acid. Salts of lithium, sodium, potassium, calcium, zinc, rubidium and cesium were obtained by classical and mechanochemical synthesis. NMR spectroscopy, UV-Vis spectrophotometry, single crystal X-ray fluorescence and diffraction were used to characterise the structure of the salts. Single-crystal and powder X-ray diffraction has enabled us to understand how the salts of 10-ethyl-10H-phenothiazine-3-carboxylic acid crystallise, and to understand the fluorescence properties of the solid state. Newly synthesised phenothiazine derivatives exhibit solid-state fluorescence, allowing the use of phenothiazine derivatives as fluorophores. The incorporation of phenothiazine derivatives into nanomaterials brings advantages in terms of fluorescence emission and extends the range of applications of

phenothiazine derivatives. The salts of 10-ethyl-10H-phenothiazine-3-carboxylic acid were incorporated into polymeric materials, with the aim of obtaining new fluorescent nanomaterials. The characterisation of the electrospun nanomaterials was carried out by TEM, SEM and FLIM microscopy, but also by fluorescence spectroscopy. The latter is used to develop a novel method for the detection of residual papillary fingerprints on different surfaces (metal, plastic, ceramic, banknotes, glass and wood). The ability of salts to retain their fluorescence in the solid state has been exploited to develop new sensors for the detection of nitro derivatives. Salts embedded in a polymer matrix acted as highly selective contrast agents for trinitrotoluene (TNT), trinitrophenol (TNP) and 4-nitrophenol.

Chapter II of the thesis includes the synthesis and characterization of new methylene blue analogous dyes, using mainly aromatic amines. Methylene blue is a phenothiazine cationic dye. It and its analogues exhibit distinct properties in photo physical, electrochemical, and biological domains. Aromatic amines were bound at the C3 and C7 positions of the phenothiazine nucleus. The chapter includes the synthesis and optical properties investigation of the methylene blue analogues, as well as the investigation of their abilities to selectively stain tumour tissue. The aim was also to optimise the synthesis methods so that, in addition to classical methods, new synthesis protocols were developed under the action of ultrasound, indirect irradiation in the ultrasonic bath or direct irradiation with the ultrasonic probe. High-resolution mass spectrometry, NMR spectroscopy, UV-Vis spectrophotometry, single-crystal fluorescence and X-ray diffraction were used for the structural elucidation of the synthesized dyes. The most effective methylene blue analogues were tested for their ability to selectively stain tissue. The most sensitive dye was also used to develop a new sensor for the determination of explosives from an unknown sample. The sensor shows increased sensitivity for trinitrophenol (TNP) and trinitrotoluene (TNT).

## **CHAPTER 1: Synthesis of 10-ethyl-10H-phenothiazine-3-carboxylic acid and its salts**

### **1.1 Introduction**

After the discovery of phenothiazine and its derivatives, these substances became the most versatile compounds in terms of applications in several fields of medicine and beyond. The extensive optical properties of phenothiazine have made it possible to use it as an organic

fluorophore. [1,2]. Most organic fluorophores exhibit high quantum fluorescence yields in solution, whereas in solids the fluorescence emission is quenched by energy transfer through intermolecular interactions [3]. In the design of fluorescent organic molecules, an important aspect is the preservation of fluorescence in a solid state. The phenothiazine used in the development of light-emitting materials, due to the non-planar "butterfly" structure exhibits fluorescence emission also in solid state. The literature describes a wide range of phenothiazine derivatives that exhibit solid-state fluorescence [4–6]. In several cases reported in the literature, solid-state fluorescence enhancement was performed by aggregate-induced emission (EIA) processes [7–9].

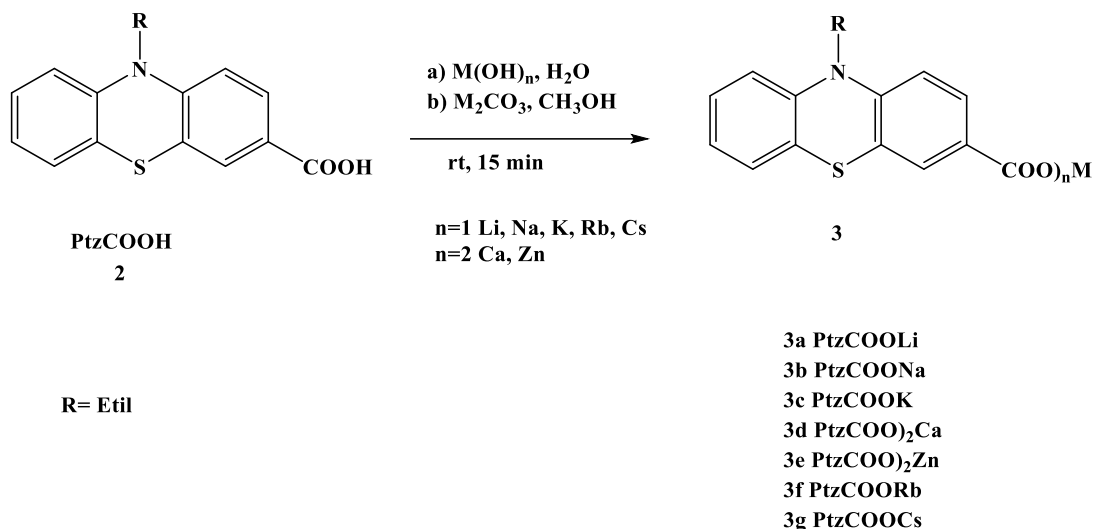
Nanofibers have properties such as porous surface and high surface-to-volume ratio, making them suitable for applications in medicine, biotechnology and sensor development. Nanomaterials can be obtained by electrospinning different polymeric materials into different fibrous assemblies. Electrospinning is a process that uses electrical force to pull charged filaments out of a polymer or molten polymer solution. The use of fluorescent nanofibers encompasses a wide range, with pharmaceutical applications [10–12], purification of ecological waste [13,14], energy storage in piezoelectric sensors [15–17], optical sensors [18], in the detection of papillary traces [19] and in the detection of nitro derivatives [20].

The application of fluorescent nanomaterials in forensics is a growing field, enabling easier and more accurate identification of crime scene evidence and the development of highly sensitive sensors to detect explosive residue [21,22].

## **1.2 Results and discussions**

### **1.2.1. Synthesis of 10-ethyl-10H-phenothiazine-3-carboxylates**

The salts of 10-ethyl-10H-phenothiazine-3-carboxylic acid, were prepared in reaction with a hydroxide or carbonate derivative (Scheme 1). In the case of the reaction with a hydroxide of alkaline metals or transitional metal hydroxide, the carboxylic acid is suspended in water, a 10% hydroxide solution is added to this suspension in drops. By this method obtained, lithium, sodium, potassium, calcium and zinc salts of 10-ethyl-10 H-phenothiazine-3-carboxylic acid were obtained. Rubidium and cesium salts were obtained by dissolving carboxylic acid in methanol and adding metal carbonate. The salts obtained by both methods were purified by recrystallisation from ethanol and reprecipitation from ethanol and diethyl ether. In addition, 10-ethyl-10H-phenothiazine-3-carboxylates can be obtained by a mechanical-chemical method.



*Scheme 1: Synthesis of salts of 10-ethyl-10H-phenothiazine-3-carboxylic acid.*

## 1.2.2. Structural characterization

### 1.2.2.1. NMR spectroscopy

In the proton spectra, the salts of 10-ethyl-10H-phenothiazine-3-carboxylic acid have two signals in the aliphatic zone and six signals in the aromatic zone. The  $^{13}\text{C}$ -NMR spectra of the 3a-g compounds contain 15 signals, of which two are in the aliphatic zone, 12 are in the aromatic zone and the carbon atom signal of the carboxylate group. The position of the carbon atom from carboxylic unit was not significantly affected by alkali and alkaline-earth metals. The  $^1\text{H}$  spectrum of the compound 3g (Figure 1) comprises the specific signals of the phenothiazine nucleus and the ethyl group. The H2 proton appears as a doublet of doublets at the chemical shift of 7.64 ppm, being characterized by the coupling constants of 8.3 Hz and 1.8 Hz. The doublet at 7.54 ppm belongs to the H4 proton having the coupling constant of 1.8 Hz. The signal of 7.14 ppm belongs to the H8 proton, having the coupling constants 8.5 Hz and 1.5 Hz, respectively. The signal at 7.12 ppm corresponds to the H6 proton, having the coupling constants of 7.6 Hz and 1.5 Hz. The signal of H9 proton is located at 6.98 ppm and exhibiting a coupling constant of 8.1 Hz. The signals of the H7 and H1 proton occur at 7.4 ppm and 8.4 ppm, respectively. The five protons of the ethyl group correspond to the two signals in the aliphatic zone, the  $\text{CH}_2$  group having a signal at 3.89

ppm a quartet with a coupling constant of 6.9 Hz, and the CH<sub>3</sub> group corresponds to the signal at 1.29 ppm, a triplet with a coupling constant of 6.9 Hz. In the <sup>13</sup>C spectrum of the 3g compound are 15 signals corresponding to the carbon atoms in the molecule. The most unveiled is the one at 168.2 ppm, which corresponds to the carbon of the carboxylate group.

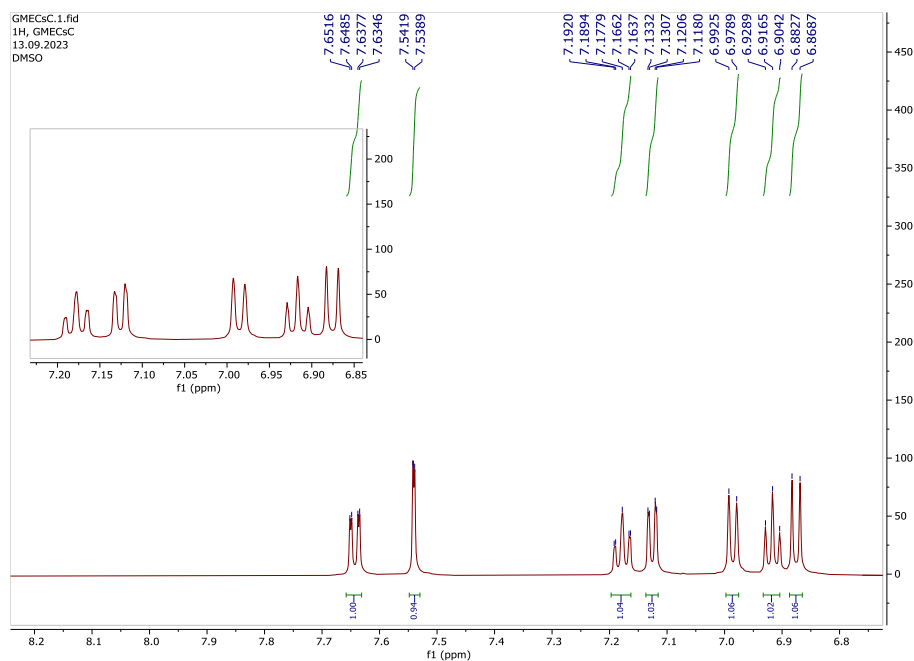


**Figure 1:** The spectrum of <sup>1</sup>H-NMR (600 MHz, dms<sub>o</sub>-d<sub>6</sub>) of 3g.

### 1.2.2.2. X-ray diffraction on single crystal

The structures of the phenothiazine carboxylic acid salts with lithium, sodium, potassium, rubidium, calcium and caesium (Figure 2-7) were studied and elucidated by x-ray diffraction on single crystals. Monocrystals were obtained by slow diffusion and slow evaporation from a wide range of organic solvents. The crystals of these salts were analysed with a SuperNova diffractometer. Experimental data collection was performed using the CrysAlis PRO software, at room temperature with CuK $\alpha$  radiation.

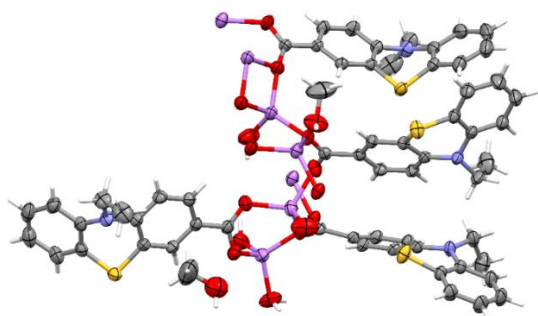


**Figure 2:** Asymmetric unit of compound **3a** presenting atoms in the form of ellipsoids at a probability level of 50%.

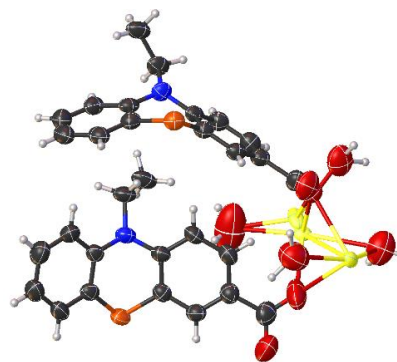


**Figure 3:** Asymmetric unit of compound **3b** presenting atoms in the form of ellipsoids at a probability level of 50%.

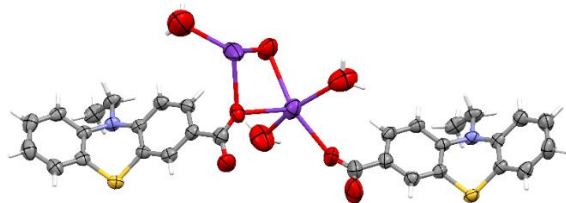


**Figure 4:** Asymmetric unit of compound **3c** presenting atoms in the form of ellipsoids at a probability level of 50%.

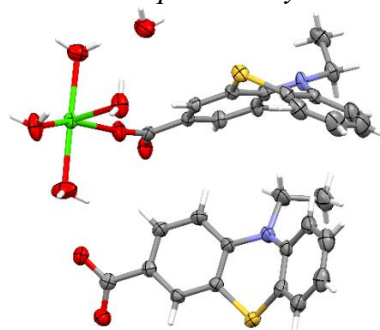


**Figure 5:** Asymmetric unit of compound **3d** presenting atoms in the form of ellipsoids at a probability level of 50%.

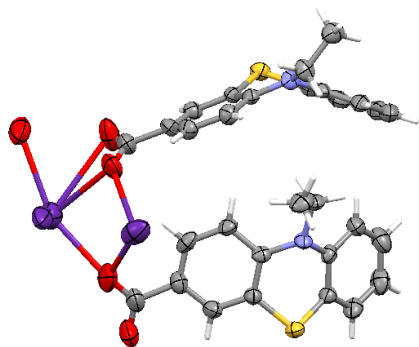


**Figure 6:** Asymmetric unit of compound **3f** presenting atoms in the form of ellipsoids at a probability level of 50%.

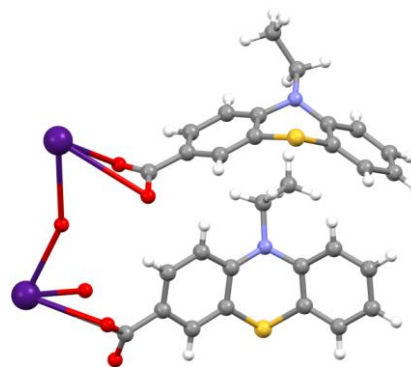


**Figure 7:** Asymmetric unit of compound **3g** presenting atoms in the form of ellipsoids at a probability level of 50%.

### 1.2.2.3. Study of electronic properties

#### 1.2.2.3.1. UV-Vis absorption spectroscopy

The salts 3a-g in water exhibit absorption bands located in the ultraviolet range at 260 nm and 313 nm respectively. (Figure 8(a) (b)). By irradiation at 260 nm in water, salts present the maximum emission between 513-518 nm. At irradiation with 313 nm the emission maximum are between 500-515 nm with the high Stokes shift at 12531cm<sup>-1</sup> in the case of derivative **3a** (Table 1).

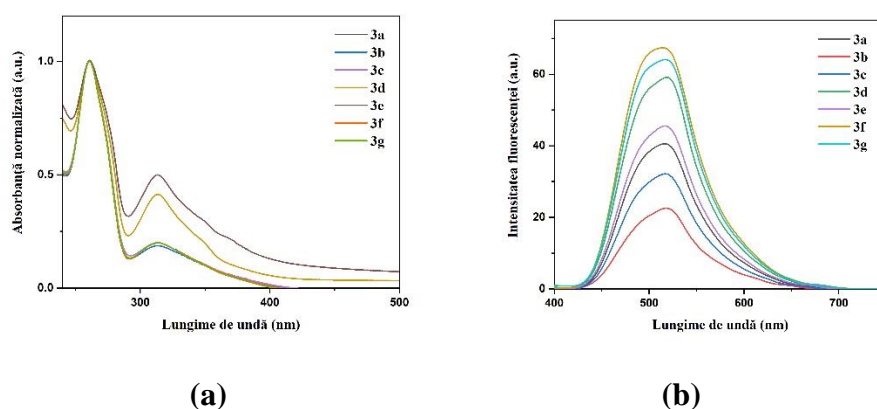


**Figure 8:** a) UV-Vis spectrum of **3a-g** salts in water, b) Fluorescence emission spectrum of **3a-g** salts in water, excitation at 260 nm.

**Table 1:** Wavelength of maximum absorption and fluorescence emission and Stokes shift of **3a-g** salts in water.

Compound	$\lambda_{abs1}$ (nm)/ $\nu$ (cm <sup>-1</sup> )	$\lambda_{em1}$ (nm)/	Stokes shift $\Delta\nu$ (cm <sup>-1</sup> )	$\lambda_{abs2}$ (nm)/ $\nu$ (cm <sup>-1</sup> )	$\lambda_{em2}$ (nm)/	Stokes shift $\Delta\nu$ (cm <sup>-1</sup> )	Quantum fluorescence yield* H <sub>2</sub> O [%]
<b>3rd</b>	260/ 3,8*10 <sup>4</sup>	516	19082	313/ 3,1*10 <sup>4</sup>	515	12531	10,8
<b>3b</b>		518	19156		501	11988	6,9
<b>3c</b>		516	19082		501	11988	7,6
<b>3d</b>		518	19156		500	11948	9,5
<b>3rd</b>		516	19082		501	11988	
<b>3f</b>		513	18968		500	11948	

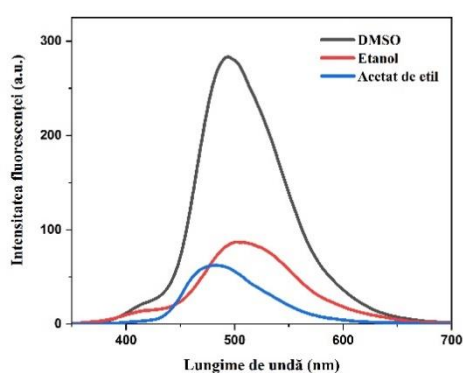
<b>3g</b>		516	19082		500	11948	

\* The absolute quantum yield of fluorescence was measured using an FP-8600 fluorescence spectrometer (Jasco, Japan) equipped with an integrating sphere (ILF-835).

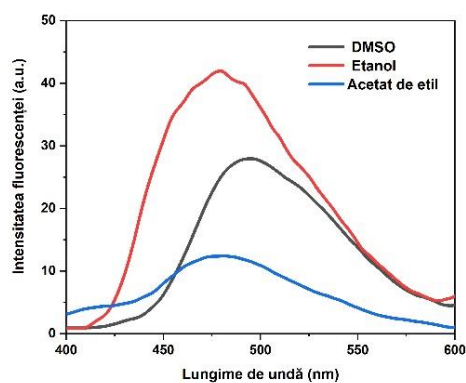
### 1.2.2.3.2. Fluorescence emission spectroscopy in solution

The polarity of the solvent does not influence the position of the fluorescence emission maxima in the case of 10-ethyl-10H-phenothiazine-3-carboxylic acid (Table 2). For compound **2** in the fluorescence emission spectrum was observed a significant hyperchromic effect in polar aprotic solvent DMSO compared to ethyl acetate and ethanol (Figure 9).

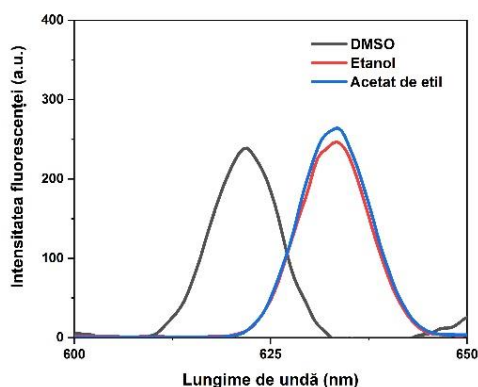
Salts of 10-ethyl-10H-phenothiazine-3-carboxylic acid exhibit blue fluorescence emission in organic solvents, with a large Stokes shift of  $16461\text{ cm}^{-1}$  for compound **3e** in ethanol and  $19156\text{ cm}^{-1}$  for compounds **3b** and **3d** in water (Table 2).



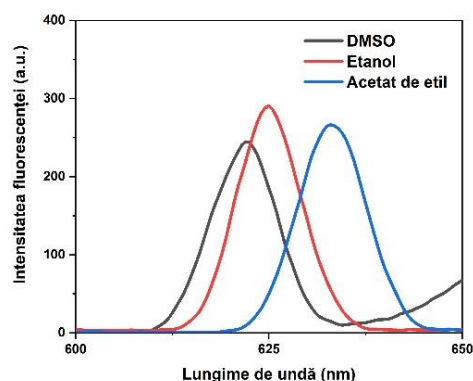
(a)



(b)



(c)



(d)

**Figure 9:** Fluorescence emission spectra for a) 10-ethyl 10H-phenothiazine-3-carboxylic acid, b) calcium salt of 10-ethyl 10H-3-carboxy-phenothiazine-3-carboxylic acid, c) zinc salt of 10-ethyl 10H-3-carboxy-phenothiazine-3-carboxylic acid, d) rubidium salt of 10-ethyl 10H-3-carboxy-phenothiazine-3-carboxylic acid, in different solvents.

**Table 2:** Wavelength of absorption maxima and fluorescence emission, extinction coefficient and Stokes shift of compound 2 and 3a-g salts in different solvents.

		<b>2</b>	<b>3rd</b>	<b>3b</b>	<b>3c</b>	<b>3d</b>	<b>3rd</b>	<b>3f</b>	<b>3g</b>
<b>DMSO</b>	$\lambda_{abs}$ (nm)	332	315	313	316	315	309	310	314
	$\lambda_{em}$ (nm)	494	484	488	483	494	621	622	449
	$\epsilon_1$ ( $\text{cm}^{-1}/\text{M}$ )	4800	1295	5076	5494	6018	3900	46000	1825
	<b>Away Stokes</b> $\Delta\nu$ ( $\text{cm}^{-1}$ )	10813	11085	11457	10942	11504	19259	16181	9576
<b>Ethanol</b>	$\lambda_{abs}$ (nm)	317	315	313	316	315	310	312	314
	$\lambda_{em}$ (nm)	505	476	505	458	479	633	624	482
	$\epsilon_1$ ( $\text{cm}^{-1}/\text{M}$ )	3800	6246	3954	9797	5406	2700	28000	1338

	<b>Away Stokes</b> $\Delta\nu$ ( $\text{cm}^{-1}$ )	11744	10738	12147	9811	10870	16461	16026	11101
<b>Ethyl acetate</b>	<b><math>\lambda_{\text{abs}}</math></b> (nm)	322	310	313	306	316	317	316	318
	<b><math>\lambda_{\text{em}}</math></b> (nm)	478	474	501	478	477	633	632	482
	<b><math>\epsilon_1</math></b> ( $\text{cm}^{-1}/\text{M}$ )	2700	6418	7105	6156	1962	1200	30000	291
	<b>Away Stokes</b> $\Delta\nu$ ( $\text{cm}^{-1}$ )	10135	11161	11988	11759	10681	15748	15823	10700

### 1.2.3. Obtaining fluorescent nanomaterials by electrospinning

Three polymer solutions were used to obtain the nanomaterials, a solution of polylactic acid (PLA) 8% dissolved in dichloromethane and chloroform, a solution of polyvinyl alcohol 5% dissolved in water and a solution of polyvinylpyrrolidone 20% dissolved in water and ethanol. Salts 3a-f were incorporated into these polymer solutions. The parameters used in the electrospinning process were optimised (Table 3); the NC-collector distance was set to the highest value when using PVP solution (NC-collector distance of 16 cm).

**Table 3:** Parameters used in the electrospinning process.

Polymer	Solvent	Mw [g/mol]	Parameters		
			Voltage [kV]	Distance AC- Collector [cm]	Flow [ $\mu\text{L}/\text{h}$ ]
8% FLAT (Polylactic acid)	DCM:Chloroform (v/v 6/8)	60 000	25	13	1500
5% PVA (Polyvinyl alcohol)	Water	89 000- 98 000	24	13	1200
20% RRP	Ethanol: Water (v/v 8/2)	40 000	16	16	500

(Polyvinylpyrrolidone)					
------------------------	--	--	--	--	--

### 1.1.1.1. Characterization of nanomaterials

#### 1.1.1.1.1. Characterization of nanomaterials by transmission electron microscopy (TEM)

The morphology of the nanomaterials obtained by electrospinning was characterised by TEM microscopy. Three different polymers were used: polyvinylpyrrolidone (PVP), polylactic acid (PLA) and polyvinyl alcohol (PVA).

The nanomaterials obtained were functionalised with fluorophores 3e and 3f. A fibrous morphology was observed in the case of the polylactic acid polymer (Figure 10(a)), a granular morphology was obtained in the case of polyvinylpyrrolidone and a typical beaded fibre morphology was obtained in the case of the PVA polymer.

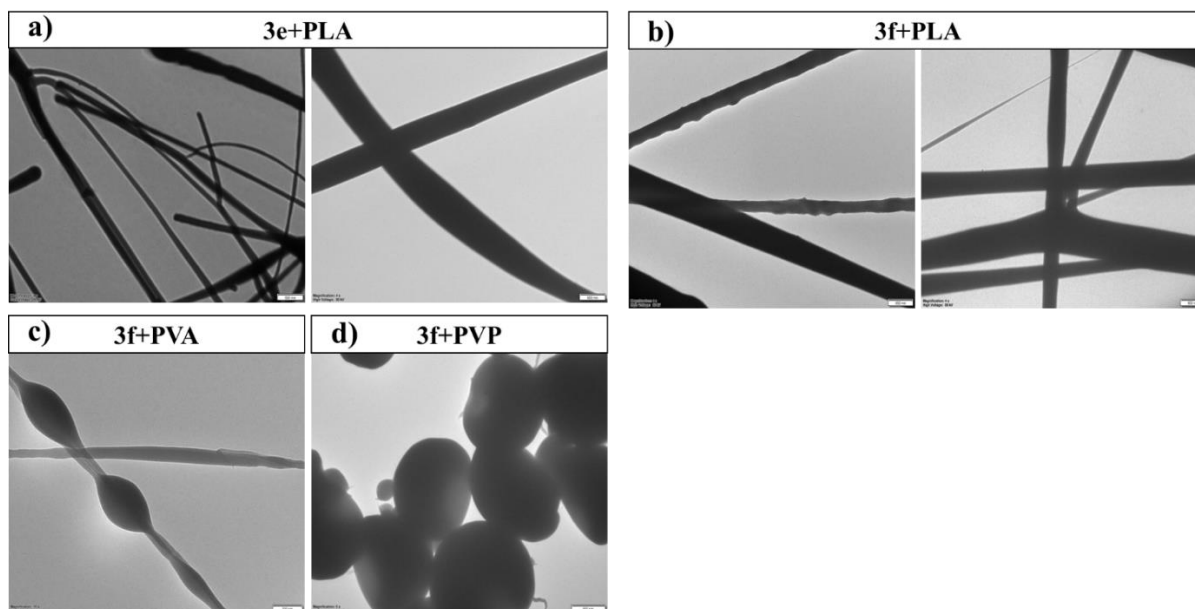


**Figure 10:** Transmission electron microscopy (TEM) images, a) TEM images of nanomaterials obtained from PLA polymer modified with fluorophore 3e; b) TEM images of nanomaterials obtained from PLA polymer modified with fluorophore 3f; c) TEM images of nanomaterials obtained from PVA polymer modified with fluorophore 3f; d) TEM images of nanomaterials obtained from PVP polymer modified with fluorophore 3f.

#### 1.1.1.1.2. Characterization of nanomaterials by scanning electron microscopy (SEM)

The morphology and diameter of the nanomaterials were characterised by scanning electron microscopy.

The nanomaterials were prepared from the PVP polymer by the electrospinning method using a voltage of 16 kV, a collector distance of 16 cm and a flow rate of 500 $\mu$ L/h. The polymer has been doped with fluorophores 3a-d. Fiber morphology was noted in the presence of sodium and potassium cations (Figure 11 b, c)), a granular morphology in the case of lithium and calcium cations (Figure 11 a, d)), for all of them, the diameter of the materials is in the nanometric range.

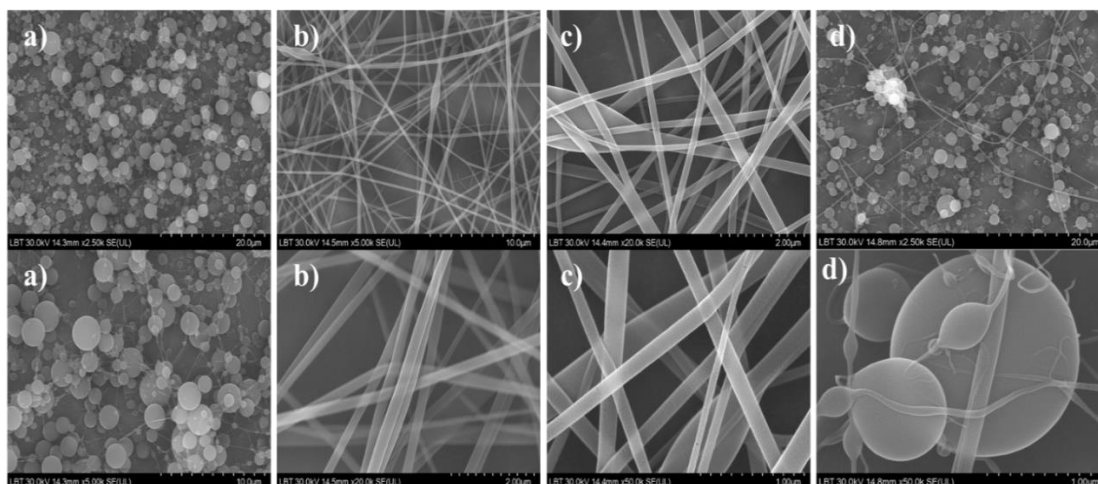


**Figure 11:** Scanning electron microscopy images a) *PVP+3a*, b) *PVP+3b*, c) *PVP+3c*, d) *PVP+3d*.

#### 1.1.1.1.3. Characterization of phenothiazine carboxylates 3a-g and nanomaterials by fluorescence imaging microscopy (FLIM)

The fluorescence lifetime for **3a-d** salts embedded in the PVP polymer were characterized by FLIM images. According to the histograms shown in Figure 12 (b), fluorophores **3a-d** exhibit intense solid-state fluorescence when excited with electromagnetic radiation at a wavelength of 375 nm. Salts **3a** and **3b** have an average fluorescence lifetime of 6 ns, while salts **3c** and **3d** have a longer fluorescence lifetime of 8.4 ns and 8.2 ns respectively (Figure 12). We can also see from the extracted histograms, the **PVP+3a**, **PVP+3b**, **PVP+3c** and **PVP+3d** complexes have a longer fluorescence lifetime than **3a-d** fluorophores. The longest lifetime displays the nanomaterials **PVP+4** (11.3 ns) and **PVP+2** (8.2 ns).

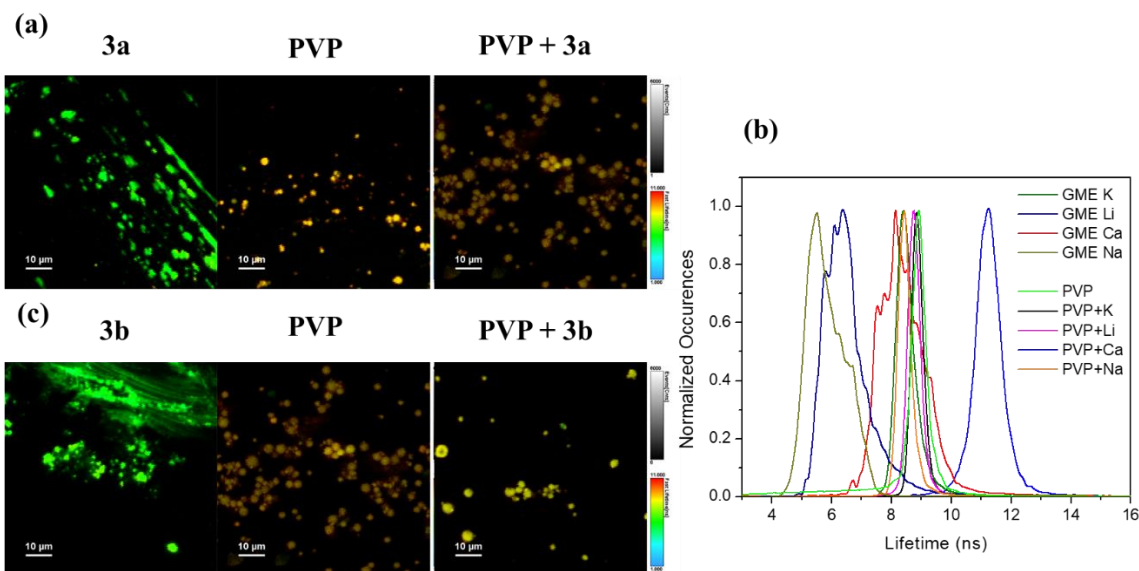


**Figure 12:** FLIM images, (a) of compound **3a**, nanomaterial obtained from PVP polymer and nanomaterial obtained from PVP modified with fluorophore **3a**, (c) **3b**, PVP and PVP + **3b**, (b) fluorescence lifetime normalized histograms. Excitation: 375 nm. The laser power is 8 μW.

## 1.2.4. Practical applications

### 1.2.4.1. Latent fingerprint detection on different surfaces

Nanomaterials obtained by electrospinning the PVP polymer modified with fluorophores **3a-d**, were used in the latent fingerprint detection from different surfaces.

#### 1.2.4.1.1. Procedure for detecting papillary traces.

The latent fingerprints were deposited by two voluntary (aged 22 and 27) on a clean different surfaces such as glass, metal (aluminium foil), polymer, polymer banknote, ceramic (ceramic mug) and wood. The sampling process is illustrated in Figure 13 and involves three simple steps, not requiring special equipment.

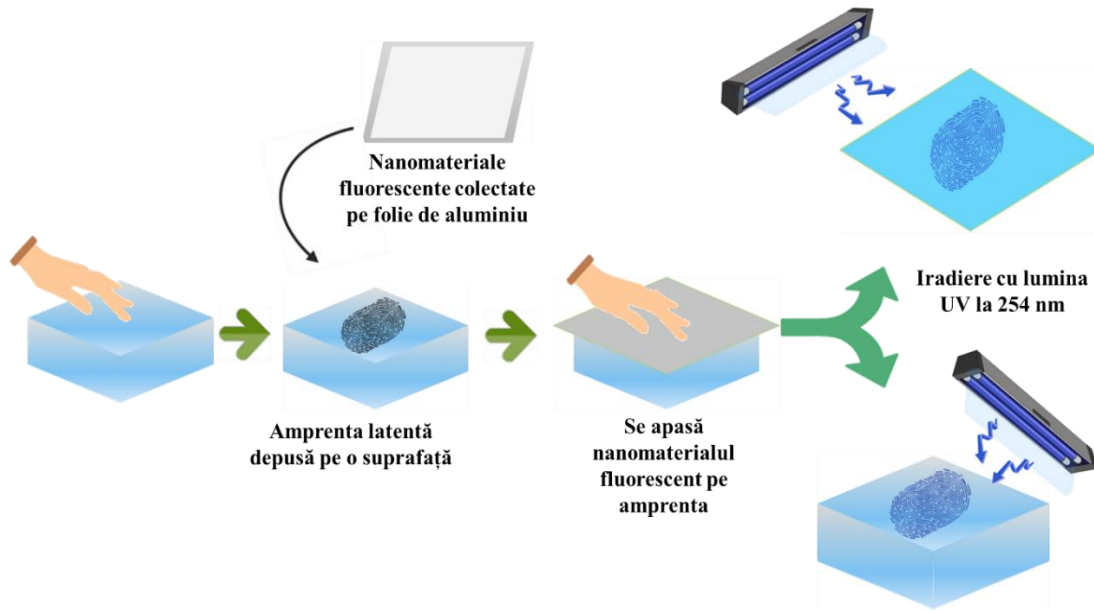
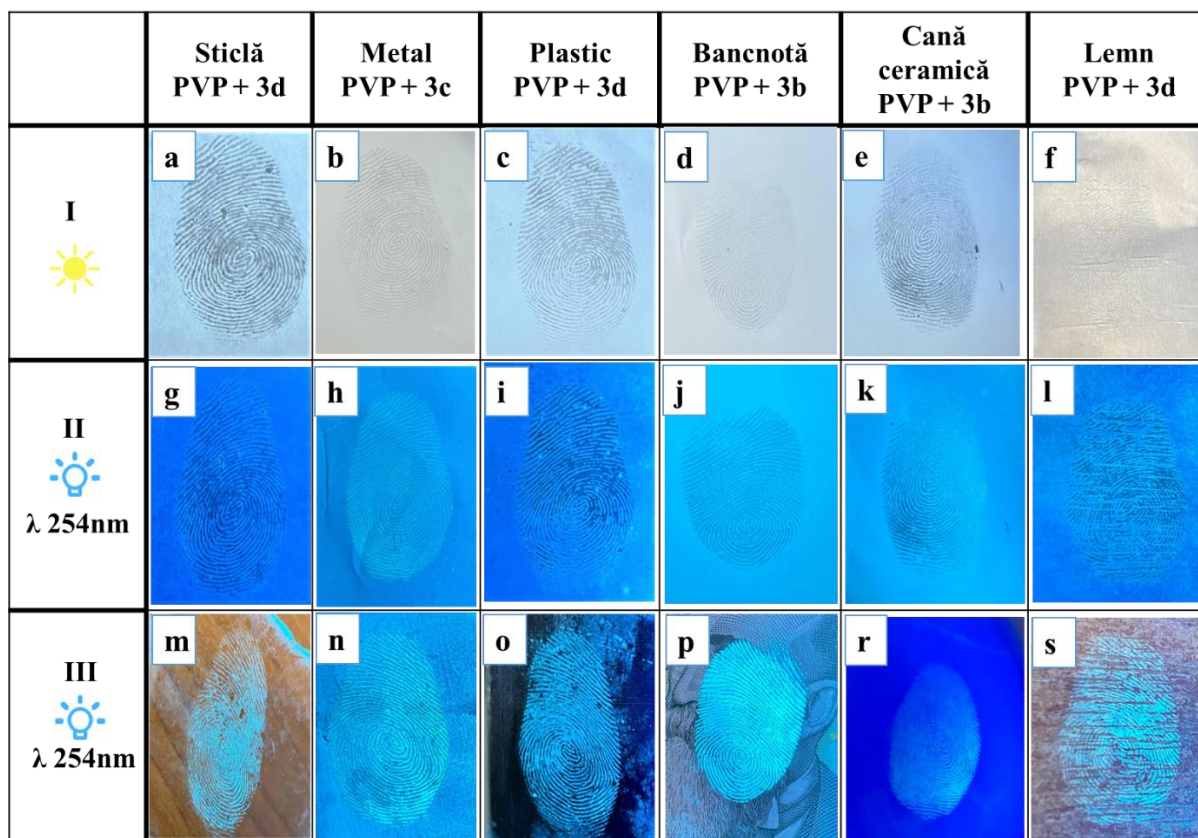


**Figure 13:** Procedure for taking latent papillary prints from a surface using fluorescent nanomaterials.

For the sampling and visualization of papillary traces, the fluorescent nanomaterials **PVP+3a**, **PVP+3b**, **PVP+3c**, **PVP+3d** were used, and the fingerprints were collected from six different surfaces (glass, metal, plastic, banknote, ceramic mug, wood). The results of latent fingerprinting are illustrated in Table 4. In the first row are presented the daylight images of the latent fingerprints transferred to the fluorescent polymer on different surfaces. In the row II, the same images can be observed, but recorded after irradiation with UV light at a wavelength of  $\lambda=254$  nm. After collecting the fingerprints with the fluorescent nanomaterial, the surfaces from which the impressions were taken are irradiated with UV light at 254 nm. Because nanomaterial traces are deposited on the surface during the sampling, papillary traces become visible during UV light irradiation, and their images are presented in Table 4, row III.

**Table 4:** Visualization of latent fingerprints taken from different surfaces. (I) Daylight images of the latent fingerprints transferred to the fluorescent polymer (**PVP+3b**, **PVP+3d**); (II) Images of latent fingerprints transferred on the surface of electrospun nanomaterials (**PVP+3b'**, **PVP+3d**) recorded following irradiation with UV light with  $\lambda=254\text{nm}$ ; (III) Visualization of latent fingerprints on different surfaces (glass, metal, plastic, banknotes, ceramics, wood) under UV light irradiation with  $\lambda=254\text{nm}$ , from the surfaces from which the fingerprints were collected.

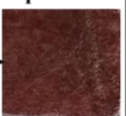
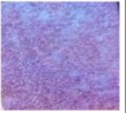


#### 1.2.4.2. Explosive Substance Detection

In order to obtain an in-depth insight into the sensor's quantitative detection the sensitivity of fluorescence emission was investigated in the presence of nitro aromatic compounds, UV-Vis absorption and fluorescence emission spectra were recorded. The change in UV-Vis absorption and fluorescence emission spectra was monitored by successive addition of nitro derivatives. Phenothiazine salts of potassium, rubidium and caesium carboxylates have been titrated in organic solvents acetone and acetonitrile with explosive substances. Compounds **3c**, **3f** and **3g** are selective for 2,4,6-trinitrotoluene (TNT), 2,4,6-trinitrophenol (TNP) and 4-nitrophenol (4-NP).

Table 5 shows the results obtained from the contamination of the sensor 1 with TNT, TNP and 4-NP, recorded with a smartphone in daylight respectively after UV irradiation. The experiments were carried out in both acetone and acetonitrile. As previously maintained, the sensor irreversibly changes colour after 10 min. In case of the sensor contamination with TNP, the response appears instantly and does not change its colour over time. In the fourth column of the table 5 we can see the response of sensor 1 in the presence of 4-NP. In this case, the colour was irreversible change after 5 min. The nitro derivative-contaminated sensor was irradiated with UV light at 254 nm. In the recorded images, a decrease in fluorescence intensities was observed.

**Table 5:** Results recorded after contamination of sensor 1 with explosives based on aromatic nitro derivatives.

	Senzor 1	Senzor 1 +TNT			Senzor 1 +TNP	Senzor 1 + 4-NP	
		30 s	După 3 min	După 10 min	30 s	30 s	După 5 min
I 							
II  $\lambda$ 365 nm							

### 1.3. Conclusions

In the first chapter of the thesis, the lithium (**3a**), sodium (**3b**), potassium (**3c**), calcium (**3d**), zinc (**3e**), rubidium (**3f**) and cesium (**3g**) salts of 10-ethyl-10H-phenothiazine-3-carboxylic acid were obtained. The structural elucidation of the synthesized salts, NMR spectroscopy methods ( $^1\text{H}$  and  $^{13}\text{C}$ ), UV-Vis and fluorescence spectrophotometry, respectively single crystal X-ray diffraction were used.

The electronic properties of compounds 3a-g were studied by UV-Vis absorption spectra, including solvatochromism in water and in organic solvents (DMSO, ethanol and ethyl acetate). The fluorescence emission properties in liquid and solid state were evaluated, all synthesised compounds exhibiting fluorescence emission both in solution and in solid state.

Following the results obtained in the characterisation of the electronic properties, the salts were incorporated into polymeric materials in order to obtain fluorescent nanomaterials by electrospinning. The nanomaterials obtained were characterised by TEM, SEM and FLIM microscopy, as well as by solid-state fluorescence spectroscopy.

For the development of forensic applications, the use of fluorescent nanomaterials derived from the polymer PVP was chosen. These nanomaterials have been successfully used to detect traces of fingerprints on various surfaces.

Another application of 10-ethyl-10H-phenothiazine-3-carboxylic acid salts is the development of sensors sensitive to aromatic nitro derivatives. The nitro derivatives to which the salts are sensitive are trinitrotoluene (TNT), trinitrophenol (TNP) and 4-nitrophenol (4-NP).

## **CHAPTER 2: Synthesis of new (N-arylamino) phenothiazinium dyes**

### **2.1. Introduction**

Phenothiazine is an organic compound discovered by Heinrich August Bernthsen in 1883 and belongs to the class of heterocyclic compounds with nitrogen and sulphur atoms derived from 1,4-thiazine. Phenothiazine and its derivatives are bioactive and have been widely used throughout history. The most prominent phenothiazine derivative is methylene blue (MB), which is highly valued for its optical properties (visible absorption/fluorescence emission). It has been investigated for a variety of applications in medicine, such as selective staining of cells or as a photosensitiser in photodynamic therapy, as well as in optoelectronics as a fluorophore in organic electrical devices or as a photosensitiser in solar cells.

MB analogues have in their structure a planar phenothiazinium chromophore system to which amino auxochrome groups (aliphatic, acyclic, cyclic or aromatic) are attached, which allows a fine regulation of their electronic properties. A redshift of the absorption maxima of MB analogues with more extensive electron conjugation is observed, compared to the parent compound, methylene blue. Analogues of methylene blue are obtained by introducing amino-auxochrome substituents in the positions C3 and C7.

### **2.2. Results and discussions**

#### **2.2.1. Synthesis of new N-arylamino phenothiazinium dyes**

Methylene blue (MB) analogues have been synthesized by introducing of amino-auxochrome units in the C3 and C7 positions of the phenazathionium unit, opening a path to the use of these methylene blue analogues in modern biomedicine for selective tumor tissue staining [23].

The most efficient strategy in the synthesis of MB analogues is the phenothiazine oxidation followed by nucleophilic substitution using aromatic amines, following the one-pot or two-pot procedures [24]. The raw material, phenothiazinium tetraiodide, was synthesized [24] by oxidation of phenothiazine with iodine in chloroform or dichloromethane solutions. MB analogues were synthesized by nucleophile substitution of the phenazathionium nucleus with amino-auxochrome groups, using the nucleophile in excess. Symmetrical cationic dyes of 3,7-di(*N*-alkyl/aryl

amino)phenothiazine, decorated with diethyl- **2a**, 4-methoxy-phenyl **2b**, 4-(2-hydroxy-ethanol)-phenyl **2c**, 3-hydroxy-phenyl **2d**, 3-chloro-phenyl **2e**, 3-bromo-phenyl **2f**, and 2-methyl-3-nitro-phenyl **2g** were obtained. To optimize the reaction conditions of **2a-g** dyes, in addition to the classical method, three alternative experimental procedures were applied: synthesis under the ultrasound irradiation, indirect irradiation in an ultrasonic bath, respectively direct irradiation with the ultrasound probe and mechanochemical synthesis.

## 2.2.2. Structural characterization

### 2.2.2.1. NMR spectroscopy

The structure of the cationic dyes (Figure 14) was characterised by NMR spectroscopy ( $^1\text{H}$  and  $^{13}\text{C}$ ) and HRMS spectrometry. In the  $^1\text{H}$ -NMR spectrum of the dyes, signals corresponding to the auxochrome groups attached at positions C3 and C7 in the aromatic zone are identified for the protons attached to the phenothiazinium nucleus, respectively.

Figure 15 shows the  $^1\text{H}$ -NMR spectrum of the **2g**, the six signals corresponding to the phenothiazinium nucleus and its substituents occur in the aromatic zone. The most shielded protons are attached to the phenothiazinium nucleus (H2 and H8); their signal appears at 8.12 ppm, as a doublet with a coupling constant of 9.2 Hz. The signal of H1 and H9 protons appear at 7.49 ppm as a doublet of doublets with coupling constants of 9.2 and 1.4 Hz, while the H4 and H6 protons correspond to the signal at 7.29 ppm. For the protons Hd and Hd' attached to the aromatic amines, the signal appear as a doublet at 7.96 ppm with a coupling constant of 8 Hz. The doublet at 7.76 ppm with a coupling constant of 7.7 Hz corresponds to the protons Hb and Hb', and the triplet at 7.60 ppm, with the coupling constant of 8.0 Hz represents the signals of the Hc and Hc' protons.

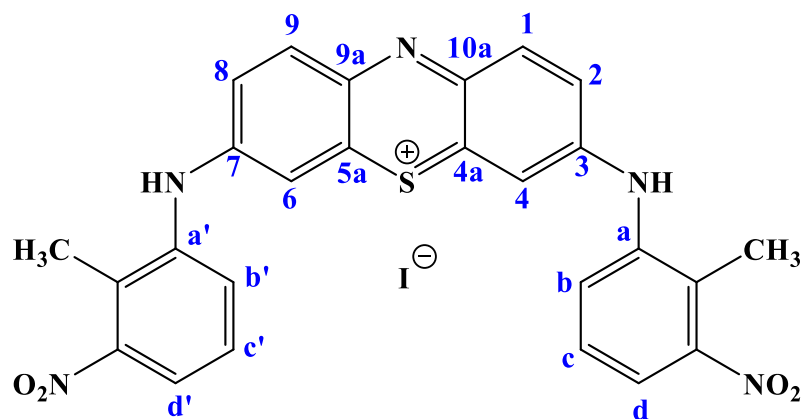


*Figure 14: Structure of compound 2g.*

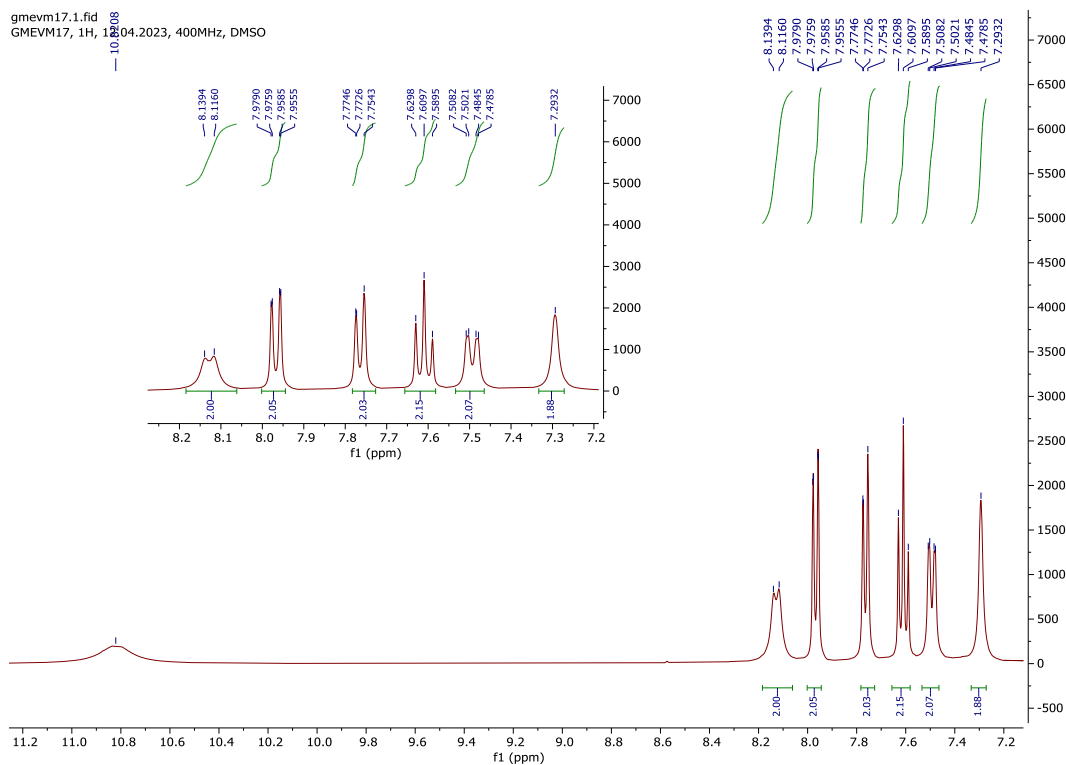


**Figure 15:**  $^1\text{H-NMR}$  (400 MHz,  $\text{DMSO-d}_6$ ) for 3,7-bis((2-methyl-3-nitrophenol)amino)phenothiazine-5-ium iodide **2g**.

### 2.2.2.2. X-ray diffraction on single crystal

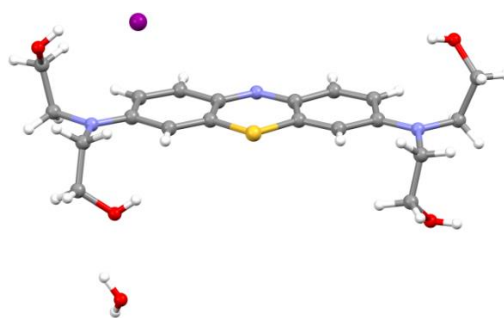


**Figure 16:** The composition of the asymmetric unit of compound **2a**.

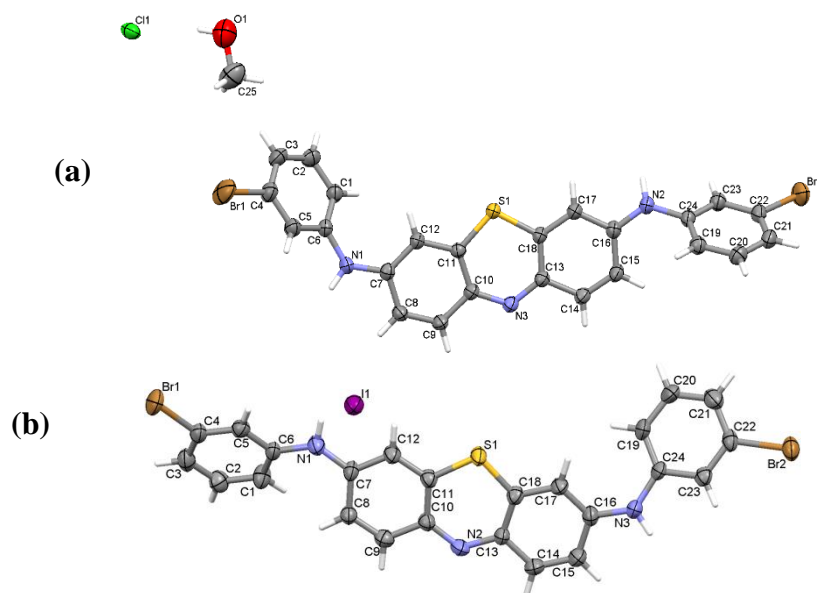


**Figure 17:** Asymmetric units of the investigated crystals illustrating atoms as thermal ellipsoids with a probability of 50%: (a) **2f-Cl** (b) **2f-I**.

### 2.2.2.3. Electronic properties

The optical properties of the synthesized dyes were investigated by recording the absorption UV-vis spectrum in solvents with different polarities. The symmetrical cationic dyes of 3,7-di(N-arylamino)-phenothiazinium (**2b-g**) exhibit absorption properties similar to methyl blue, with absorption maxima in the visible range between 547 nm and 683 nm, with increased values of the molar extinction coefficient ( $\log \epsilon$  in the range of 4.19-4.97). A reduced solvatochromism was observed in the solvents with different polarities (Figure 17).

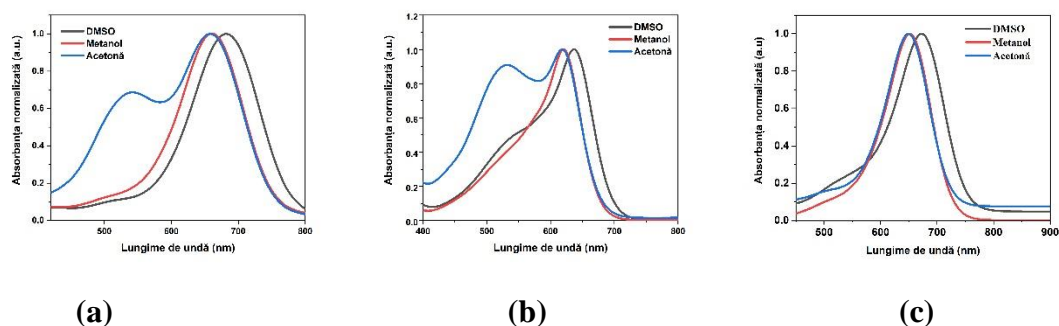


**Figure 18:** Normalized UV-vis absorption spectra of the compounds **2d** (a), **2g** (b), and **2f** (c) in different solvents.

### 2.2.3. Characterization of 2b-f dyes by FLIM imaging

The study of optical properties confirmed that only dye **2c** display the fluorescence in organic solvents, but by FLIM microscopy of dyes **2b-f** in solid state proved the fluorescence emission properties of this compound in solid state. The samples were excited at 640 nm, and the results are shown in the OPE-FLIM images in Figure 18. The most intense fluorescence was recorded for compound **2c**, which is characterized by a fluorescence emission lifetime of 0.56 ns. The longest lifetime of fluorescence emission was recorded for dyes **2b** and **2e**, being characterized by a fluorescence lifetime of 0.96 ns (Figure 19).

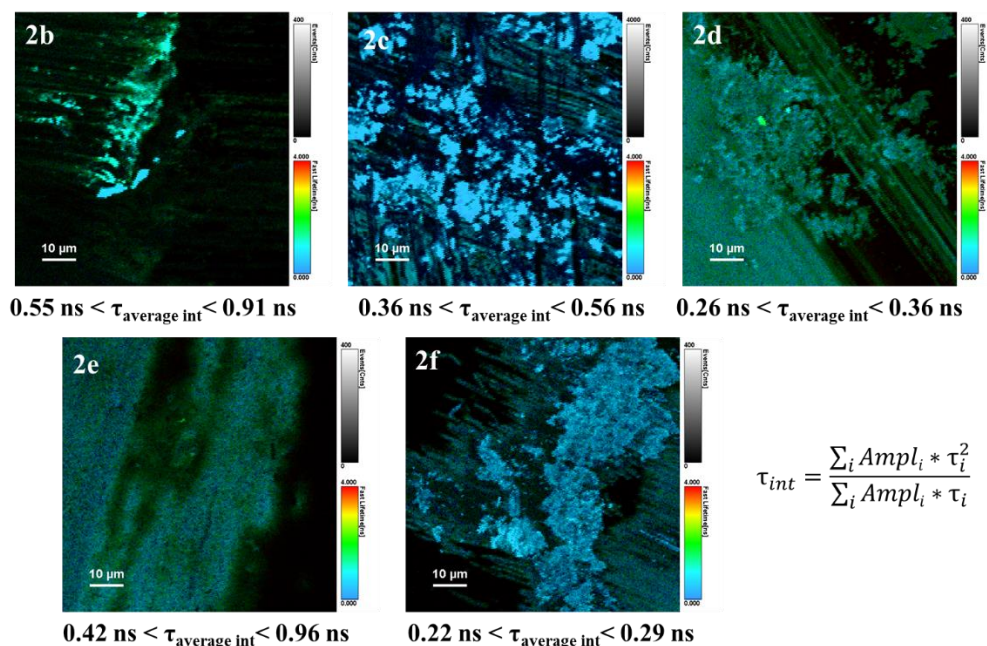


**Figure 19:** OPE-FLIM images of **2b-f** dyes in solid state, excitation at 640 nm and at 5.6 μW.

### 2.2.4. Practical applications

#### 2.2.4.1. Explosive Substance Detection

The dye **2f** was used to develop sensors sensitive to nitro derivatives. For obtaining sensor having incorporated dye **2f**, the steps described in the previous chapter were followed. The polyethylene terephthalate polymer was used as a sensor support and the dip-coating process was employed for sensor fabrication. In order to determine the interaction of the dye with the nitro

derivatives, the changes in the UV-vis spectra after successive titrations with TNT and TNP were monitored.

Figure 20 shows how to use the **2f** sensor in the presence of nitro derivatives. The colour change is monitored by dripping samples containing nitro derivatives onto the surface of the sensor. When the sensor is contaminated with TNT, the dye changes to the quinonimine form, which is associated with a change in colour from blue to pink-purple. From the moment of contamination, the colour of the sensor changes completely after 10 minutes. In the presence of TNP, the sensor colour changes from blue to green, which is also confirmed by UV-vis spectroscopy, with the appearance of an absorption band at 869 nm (Table 6).

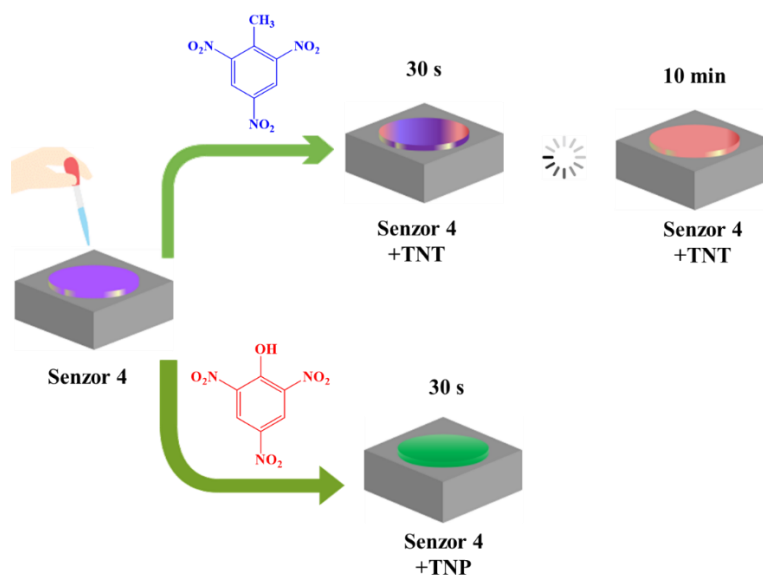


**Figure 20:** How to use sensor 4 in the presence of TNT nitro derivatives, and TNP.

**Table 6:** Results obtained from **2f** sensor contamination with TNT and TNP (dye concentration  $1.6 \cdot 10^{-3} M$ ).

	Senzor 4	Senzor 4 + TNT			Senzor 4+ TNP
I					
		30 s	După 3 min	După 10 min	30 s

### 2.2.4.2. Dyes applications in cells staining

After preliminary lipophilicity tests and FLIM imaging (Figure 21), four dyes (**2d-g**) were selected to investigate their ability to stain human retinal pigment epithelial D407 cells. The fluorophores used reduced cell viability by 34-40% for dye **2d**, 45-50% for dye **2f**, 46-53% for dye **2g** and 44% for dye **2e**. Analysis of the results showed that cell cytotoxicity was concentration dependent, except for dye **2e** which showed no significant changes compared to the control sample. It was also found that the cytoplasm is selectively stained by the use of **2d-g** fluorophores.

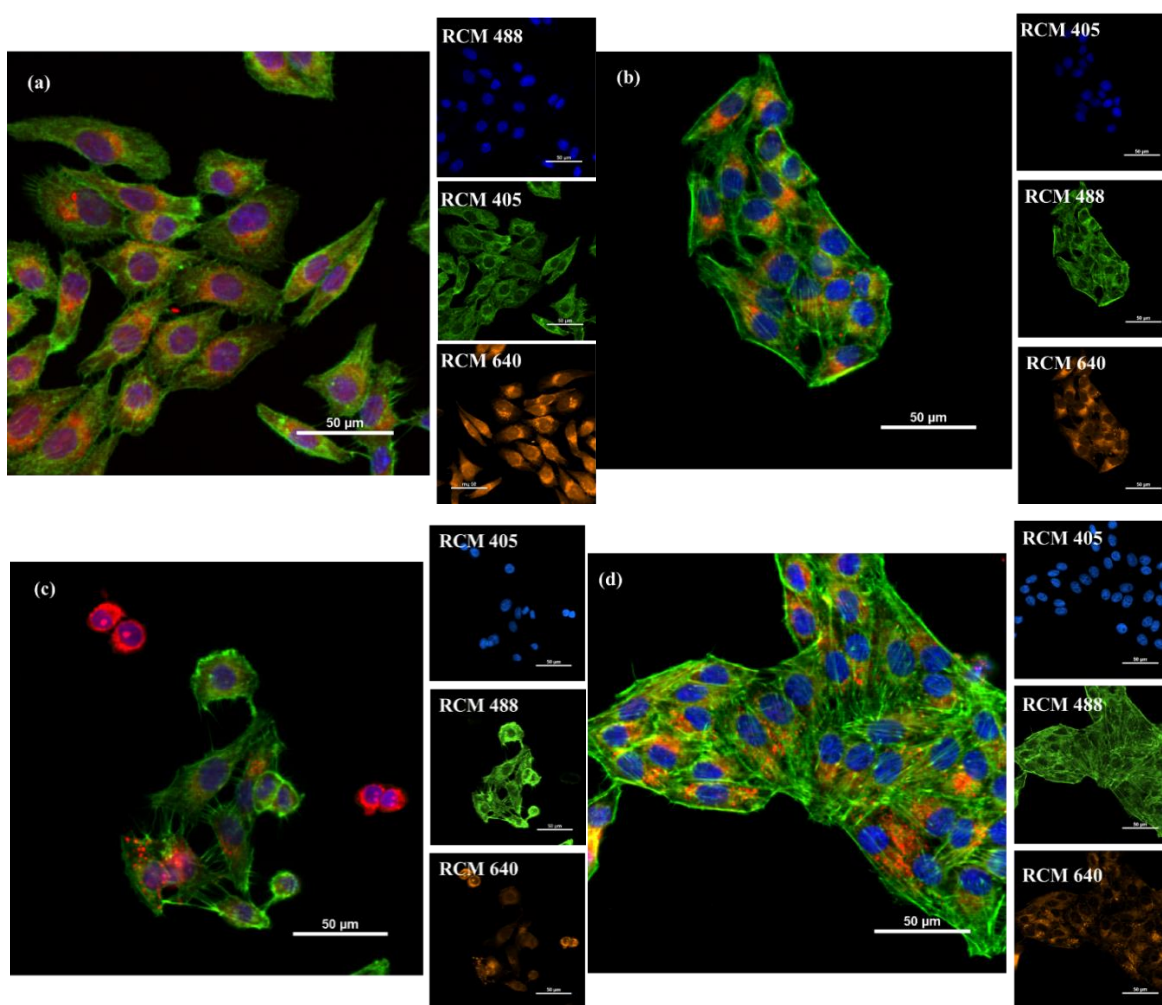


**Figure 21:** Rescan confocal microscopy (RCM) images, collected after excitation at different wavelengths: 405 nm (for DAPI dye), 488 nm (for green fluorescence protein) and 640 nm for **4b-f** dyes, respectively, used on human retinal pigment epithelial cells D407, a) **4d** dye; (b) **4f**; (c) **4g**; (d) **4f**.

### 2.3. Conclusions

This chapter presents the synthesis of dye analogues of methyl blue, including seven new dyes. Methylene blue analogues have been synthesised by introducing amino-auxochromic groups at the C3 and C7 positions of the phenazathionium nucleus.

More efficient synthetic methods were identified and reaction conditions were optimised. In addition to the classical reaction method, alternative experimental procedures have been developed: ultrasound-assisted synthesis with indirect and direct irradiation and mechanochemical synthesis in the case of dye 2a.

Cationic dyes containing the phenazathionium chromophore symmetrically substituted at positions C3 and C7 have been obtained by introducing amino groups such as diethylanol 2a, 4-methoxy-phenyl 2b, 4-(2-hydroxy-ethanol)-phenyl 2c, 3-hydroxy-phenyl 2d, 3-chloro-phenyl 2e, 3-bromo-phenyl 2f and 2-methyl-3-nitro-phenyl 2g.

The quinonimine neutral dyes form of methylene blue analogues decorated with 4-methoxy-phenyl **4b**, 4-(2-hydroxy-ethanol)-phenyl **4c**, 3-hydroxy-phenyl **4d**, 3-chloro-phenyl **4e**, 3-bromo-phenyl **4f**, and 2-methyl-3-nitro-phenyl **4g** were obtained.

By nucleophilic substitution of 2-chlorophenazathionium tetraiodide with aromatic amines, dyes containing amino auxochrome units decorated with 4-methoxy-phenyl **3b**, 3-hydroxy-phenyl **3d**, 3-chloro-phenyl **3e**, 3-bromo-phenyl **3f**, and 2-methyl-3-nitro-phenyl **3g** groups were synthesised.

The structural assignments of the synthesized dyes, high-resolution mass spectrometry, NMR spectroscopy, UV-vis absorption spectrophotometry and fluorescence emission, respectively single-crystal X-ray diffraction methods were used. The most efficient analogues of methyl blue analogues have been selected for *in vitro* testing of their ability to selectively stain epithelial tissue. A series of dye properties of the were determined, such as lipophilicity photodynamic stability and the tendency to aggregate in the solution; were investigated by UV-Viz spectroscopy. The ability of the dye to internalise into cells and its distribution in the cellular environment were analysed by fluorescence microscopy.

A new sensor was also developed using dye 2f for the detection of explosives from an unknown sample. The sensor shows good sensitivity for trinitrophenol (TNP) and trinitrotoluene (TNT).

## References

- [1] Moll B, Tichelkamp T, Wegner S, Francis B, Müller TJJ, Janiak C. Near-infrared (NIR) surface-enhanced Raman spectroscopy (SERS) study of novel functional phenothiazines for potential use in dye sensitized solar cells (DSSC). *RSC Adv* 2019; 9:37365–75. <https://doi.org/10.1039/c9ra08675g>.
- [2] Mayer L, May L, Müller TJJ. The interplay of conformations and electronic properties in: N -aryl phenothiazines. *Org Chem Front* 2020; 7:1206–17. <https://doi.org/10.1039/d0qo00182a>.
- [3] Rao M R, Liao CW, Su WL, Sun SS. Quinoxaline based D-A-D molecules: High contrast reversible solid-state mechano- and thermo-responsive fluorescent materials. *J Mater Chem C* 2013; 1:5491–501. <https://doi.org/10.1039/c3tc31179a>.
- [4] Ramachandran E, Vandarkuzhali SAA, Sivaraman G, Dhamodharan R. Phenothiazine Based Donor–Acceptor Compounds with Solid-State Emission in the Yellow to NIR Region and Their Highly Selective and Sensitive Detection of Cyanide Ion in ppb Level. *Chem - A Eur J* 2018; 24:11042–50. <https://doi.org/10.1002/chem.201800216>.
- [5] Stoean B, Rugina D, Focsan M, Craciun AM, Nistor M, Lovasz T, et al. Novel (Phenothiazinyl)vinyl-pyridinium dyes and their potential applications as cellular staining agents. *Int J Mol Sci* 2021; 22:1–21. <https://doi.org/10.3390/ijms22062985>.
- [6] Gaina L, Torje I, Gal E, Lupan A, Bischin C, Silaghi-Dumitrescu R, et al. Microwave assisted synthesis, photophysical and redox properties of (phenothiazinyl)vinyl-pyridinium dyes. *Dye Pigment* 2014; 102:315–25. <https://doi.org/DOI 10.1016/j.dyepig.2013.10.044>.
- [7] Ana AC, Pina J, Seixas de Melo JS. Structure-relation properties of N-substituted phenothiazines in solution and solid state: Photophysical, photostability and aggregation-induced emission studies. *J Mol Liq* 2020;317:113966. <https://doi.org/10.1016/j.molliq.2020.113966>.
- [8] Chen Y, Xu C, Xu B, Mao Z, Li JA, Yang Z, et al. Chirality-activated mechanoluminescence from aggregation-induced emission enantiomers with high contrast mechanochromism and force-induced delayed fluorescence. *Mater Chem Front* 2019;

3:1800–6. <https://doi.org/10.1039/c9qm00312f>.

- [9] Paquin F, Rivnay J, Salleo A, Stingelin N, Silva C. Multi-phase semicrystalline microstructures drive exciton dissociation in neat plastic semiconductors. *J Mater Chem C* 2015; 3:10715–22. <https://doi.org/10.1039/b000000x>.
- [10] Kazsoki A, Szabó P, Domján A, Balázs A, Bozó T, Kellermayer M, et al. Microstructural Distinction of Electrospun Nanofibrous Drug Delivery Systems Formulated with Different Excipients. *Mol Pharm* 2018; 15:4214–25. <https://doi.org/10.1021/acs.molpharmaceut.8b00646>.
- [11] Wei Z, Zhao W, Wang Y, Wang X, Long S, Yang J. Novel PNIPAm-based electrospun nanofibres used directly as a drug carrier for "on-off" switchable drug release. *Colloids Surfaces B Biointerfaces* 2019;182:110347. <https://doi.org/10.1016/j.colsurfb.2019.110347>.
- [12] Singh B, Garg T, Goyal AK, Rath G. Development, optimization, and characterization of polymeric electrospun nanofiber: a new attempt in sublingual delivery of nicorandil for the management of angina pectoris. *Artif Cells, Nanomedicine Biotechnol* 2016; 44:1498–507. <https://doi.org/10.3109/21691401.2015.1052472>.
- [13] Yang D, Li L, Chen B, Shi S, Nie J, Ma G. Functionalized chitosan electrospun nanofiber membranes for heavy-metal removal. *Polymer (Guildf)* 2019; 163:74–85. <https://doi.org/10.1016/j.polymer.2018.12.046>.
- [14] Shekh MI, Patel DM, Patel KP, Patel RM. Electrospun nanofibers of poly(NPEMA-co.-CMPMA): Used as Heavy metal ion remover and water sanitizer. *Fibers Polym* 2016; 17:358–70. <https://doi.org/10.1007/s12221-016-5861-9>.
- [15] Cai Z, Xiong P, He S, Zhu C. Improved piezoelectric performances of highly oriented poly( $\beta$ -hydroxybutyrate) electrospun nanofiber membrane scaffold blended with multiwalled carbon nanotubes. *Mater Lett* 2019; 240:213–6. <https://doi.org/10.1016/j.matlet.2019.01.010>.
- [16] Baniasadi M, Xu Z, Cai J, Daryadel S, Quevedo-Lopez M, Naraghi M, et al. Correlation of annealing temperature, morphology, and electro-mechanical properties of electrospun

- piezoelectric nanofibers. *Polymer (Guildf)* 2017; 127:192–202.  
<https://doi.org/10.1016/j.polymer.2017.08.053>.
- [17] Zhao Z, Li B, Xu L, Qiao Y, Wang F, Xia Q, et al. A sandwich-structured piezoresistive sensor with electrospun nanofiber mats as supporting, sensing, and packaging layers. *Polymers (Basel)* 2018; 10:1–13. <https://doi.org/10.3390/polym10060575>.
- [18] Camposeo A, Moffa M, Persano L. Electrospun fluorescent nanofibers and their application in optical sensing. *Nanosci Technol* 2015; 96:129–55.  
[https://doi.org/10.1007/978-3-319-14406-1\\_6](https://doi.org/10.1007/978-3-319-14406-1_6).
- [19] Mazzini Júnior EG, de Almeida Cantalice JD, de Assis AML, Duarte de Freitas J, Manzine Costa LM, Santos Ribeiro A. Fluorescent polymer nanofibers based on polycaprolactone and dansyl derivatives for development of latent fingerprints. *J Appl Polym Sci* 2020; 137:12–5. <https://doi.org/10.1002/app.49804>.
- [20] Eddin MZ, Zhilina EF, Chuvashov RD, Dubovik AI, Mekhaev A V., Chistyakov KA, et al. Synthesis of random copolymers of styrene and arylamino substituted styrenes and their sensitivities towards nitroaromatics. *J Appl Polym Sci* 2024; 141:1–21.  
<https://doi.org/10.1002/app.55355>.
- [21] Mathur S, SK C. Effect of Disguise on Fundamental Frequency of Voice. *J Forensic Res* 2016;7. <https://doi.org/10.4172/2157-7145.1000327>.
- [22] Pooja A. A Developmental Overview of Voice as a Steadfast Identification Technique. *J Forensic Res* 2015;06. <https://doi.org/10.4172/2157-7145.1000282>.
- [23] Wainwright M. The use of dyes in modern biomedicine. *Biotech Histochem* 2003; 78:147–55. <https://doi.org/10.1080/10520290310001602404>.
- [24] Padnya PL, Khadieva AI, Stoikov II. Current achievements and perspectives in synthesis and applications of 3,7-disubstituted phenothiazines as Methylene Blue analogues. *Dye Pigment* 2022;208:110806. <https://doi.org/10.1016/j.dyepig.2022.110806>.